Published in final edited form as:
Immunity. 2009 October 16; 31(4): 632–642. doi:10.1016/j.immuni.2009.09.004.

Kinetics of early TCR signaling regulate the pathway of lytic granule delivery to the secretory domain

Allison M. Beal[¶], **Nadia Anikeeva**[¶], **Rajat Varma**[†,‡], **Thomas O. Cameron**[†], **Gaia Vasiliver-Shamis**[†], **Philip J. Norris**[§], **Michael L. Dustin**[†], and **Yuri Sykulev**[¶,#]

[¶] Department of Microbiology and Immunology and Kimmel Cancer Institute, Thomas Jefferson University, Philadelphia, PA19107

[†] Helen L and Martin S Kimmel Center for Biology and Medicine of the Skirball Institute of Biomolecular Medicine, New York University School of Medicine, New York, NY 10016

[§] Blood Systems Research Institute and the Departments of Laboratory Medicine and Medicine, University of California, San Francisco, CA 94118

SUMMARY

Cytolytic granule mediated killing of virus-infected cells is an essential function of cytotoxic T lymphocytes. Analysis of lytic granule delivery shows that the granules can take long or short paths to the secretory domain where they are released. Both paths utilize the same intracellular molecular events, which have different spatial and temporal arrangements in each path and are regulated by the kinetics of downstream Ca^{2+} mediated signaling. Rapid and robust signaling causes swift granule concentration near the MTOC and subsequent delivery by the polarized MTOC directly to the secretory domain - the shortest and fastest path. Indolent signaling leads to late recruitment of granules that move along microtubules to the periphery of the synapse and then move tangentially to fuse at the outer edge of the secretory domain - a longer path. The short pathway is associated with faster granule release and more efficient killing than the long pathway.

Keywords

Cytotoxic T lymphocytes; TCR early signaling; kinetics of Ca^{2+} signaling; cytolytic granules; immunological synapse

INTRODUCTION

$CD8^+$ CTL exercise cytolytic activity and play a central role in the destruction of virus-infected cells (Brander et al., 2006; McMichael, 2006). Cytolytic activity is mediated by the vectoral release of the lytic granules toward the target cell through a cytolytic synapse. The cytolytic synapse is organized into a central secretory domain surrounded by a ring of adhesion molecules (Anikeeva et al., 2005; Potter et al., 2001; Somersalo et al., 2004; Stinchcombe et al., 2001), analogous to the central supramolecular activation cluster (cSMAC) and peripheral

#Corresponding author: Yuri Sykulev, Department of Microbiology and Immunology, Kimmel Cancer Center, BLSB 706, Thomas Jefferson University, Philadelphia, PA 19107, Phone: 215-503-4530, Fax: 215-923-4153, ysykulev@lac.jci.tju.edu.
‡Present address: NIAID/LCMI, National Institutes of Health, Bldg 4, Rm 431, 4 Center Drive, Bethesda, 20892

supramolecular activation cluster (pSMAC) in helper $CD4^+$ T cell immunological synapses (IS) (Grakoui et al., 1999; Monks et al., 1998). The polarization of the lytic granules to the cytolytic synapse occurs within minutes of TCR stimulation and the granules can be directly delivered by the microtubule organizing center (MTOC) to an F-actin depleted zone of plasma membrane within the cSMAC (Stinchcombe and Griffiths, 2007). MTOC mediated delivery has been seen in CTL stimulated by either allogeneic target cells or anti-CD3 antibodies that induce a very strong TCR signaling. Granules can also move from the periphery along microtubules that are oriented tangentially to the synapse and fuse with the plasma membrane (Poenie et al., 2004). What mechanism controls the granule delivery pathway to the synapse and whether it is associated with the kinetics of granule release is not known.

Serine esterases, a major component of cytolytic granules in $CD8^+$ CTL, are also found in $CD4^+$ T cells (Pasternack et al., 1986) suggesting that these cells have a potential to exercise cytolytic activity. Although the role of $CD4^+$ CTL is not well understood, they are found during chronic viral infections (Appay et al., 2002; Heller et al., 2006; Norris et al., 2001) and typically are less potent lytic effectors than $CD8^+$ CTL (Hahn et al., 1995). Recently, we have shown that $CD4^+$ CTL form unstable cytolytic synapses, accounting for about a third of the difference in potency between $CD4^+$ and $CD8^+$ CTL (Beal et al., 2008). However, the majority of the difference in efficiency between $CD8^+$ and $CD4^+$ CTL appears to result from additional unidentified factors. Since both CTL produce equal amounts of cytolytic granules with similar potency (Beal et al., 2008), we thought that the unknown mechanistic components accounting for the different efficiency of lysis by these CTL may be related to variations in granule delivery mechanism. We also thought that comparison of the same CTL clone responding to strong and weak agonists would provide additional opportunity to further evaluate these differences.

To learn more about the mechanism controlling granule delivery, we analyzed the pattern of granule polarization at the CTL contact surface, kinetics of granule release in a real time scale and the kinetics of intracellular Ca^{2+} accumulation as a measure of early TCR signaling. We have shown that lytic granules can take either a short or long path to the cytolytic synapse resulting in distinct patterns of granule polarization. More effective CTL polarized granules at the center of the synapse, whereas the granules in less effective CTL were mostly seen over the pSMAC. Nevertheless, granule release was always evident within the cSMAC, but the release by CTL responding with lesser efficiency was delayed. We have demonstrated that the pattern of granule polarization and release kinetics are linked to differences in kinetics of intracellular Ca^{2+} signaling in the CTL. These data provide evidence for a model in which the kinetics of downstream Ca^{2+} signaling regulate differences in the spatial and temporal arrangements of the same molecular hardware to determine the path of granule delivery.

RESULTS

Different polarization patterns of cytolytic granules at cytolytic synapses

We compared the recruitment pattern of cytolytic granules in $CD4^+$ and $CD8^+$ CTL by visualizing granule polarization relative to the cSMAC and pSMAC at the CTL-bilayer interface. Three-dimensional imaging revealed that granules were polarized towards the cell-bilayer interface similarly in both $CD4^+$ and $CD8^+$ CTL (Fig. S1). However, less effective $CD4^+$ CTL positioned granules over the pSMAC region (Fig. 1A) and failed to accumulate granules in the cSMAC even after the cells interacted with bilayers for up to 40 minutes (not shown). While $CD8^+$ CTL positioned their granules over the cSMAC within less than 5 minutes, the granules were equally distributed between the cSMAC and the pSMAC, and the fraction of the granules in the pSMAC increased with time (Fig. 1A).

We also analyzed granule distribution in CTL that formed conjugates with target cells bearing cognate pMHC ligands and found that the granules were concentrated within the cSMAC

surrounded by a peripheral actin ring in the vast majority of $CD8^+$ CTL (Fig. 1B). In contrast, polarized granules in less effective $CD4^+$ CTL were scattered near the peripheral actin ring even though the target cells presented a very high density of cognate pHLA-DR1 ligands.

Location of polarized granules within cytolytic synapses depends on the strength of TCR stimulation

To evaluate the effect of the strength of TCR stimulation on the pattern of granule distribution at the synapse we varied the strength of TCR/pMHC/co-receptor interactions in $CD8^+$ and $CD4^+$ CTL.

To examine the contribution of co-receptor-MHC interaction, we utilized a mutant HLA-A2 (A245V), which is defective in binding to the CD8 co-receptor (Anikeeva et al., 2006; Gao and Jakobsen, 2000) but is loaded with agonist peptide. To vary the strength of TCR-pMHC interactions, we tested a weak agonist pMHC ligand (IV9-A7-HLA-A2) containing intact HLA-A2. Exposure of $CD8^+$ CTL to bilayers loaded with mutant HLA-A2(A245V) complexes loaded with cognate peptide revealed lytic granule accumulation in the pSMAC that resembles the pattern observed with $CD4^+$ CTL (Fig. 1C). TCR stimulation with weak agonist IV9-A7-HLA-A2 complexes in the bilayers also altered the central granule location similar to that observed with mutant HLA-A2 complexes (Fig. 1C).

We further varied the strength of TCR engagement by decreasing the density of strong agonist pMHC on the bilayers. At the lowest density of the pMHC, which was still sufficient to induce cytolytic synapse formation and granule polarization, granules were distributed within cytolytic synapse of $CD8^+$ CTL similar to that observed for $CD4^+$ CTL Fig. S2). Nevertheless, $CD4^+$ CTL were not able to concentrate the granules in the cSMAC even at high densities of pMHC (500 molecules/μm^2) on the bilayers (Fig. 1A) or after conjugation with target cells sensitized at high peptide concentration (10^{-5} M) (Fig. 1B).

To increase the strength of TCR engagement of $CD4^+$ CTL we resorted to anti-CD3 antibodies that mimic strong TCR engagement. The antibodies were incorporated into ICAM-1 containing bilayers to stimulate $CD4^+$ CTL. We found that anti-CD3 antibodies induced lytic granule accumulation in the cSMAC in $CD4^+$ CTL (Fig. S3). In control experiments, polarized granules in $CD8^+$ CTL exposed to bilayers containing anti-CD3 antibodies and ICAM-1 were also located in the cSMAC (Fig. S3).

These data demonstrate that the ability to accumulate granules in the central domain of cytolytic synapses is intact in both $CD4^+$ and $CD8^+$ CTL and is controlled by the strength of TCR/pMHC/co-receptor interactions.

Granule location in the cytolytic synapse does not correlate with the magnitude of TCR mediated signaling

To evaluate the intensity of TCR signaling in $CD4^+$ and $CD8^+$ CTL we measured Ca^{2+} flux induced by live target cells sensitized with various concentrations of cognate peptides. There was a difference in the dependence of the magnitude of Ca^{2+} response upon the peptide concentration for $CD4^+$ and $CD8^+$ CTL (Fig. S4), consistent with the different sensitivity of target cell lysis and granule release by these CTL (Beal et al., 2008). However, at a high concentration of cognate peptides we observed a very similar magnitude in intracellular Ca^{2+} accumulation in both $CD4^+$ and $CD8^+$ CTL (Fig. S4 and Fig. S5) despite very different patterns of granule polarization by these CTL (Fig. 1B).

In contrast to Ca^{2+} flux, TCR membrane proximal signaling occurs in the vicinity of engaged TCR and leads to the assembly of large signaling complexes often called signalosomes (Werlen and Palmer, 2002). To probe the proximal membrane signaling we utilized total internal

reflection fluorescence (TIRF) imaging of activated Src kinases at the CTL/bilayer interface. After 2 minutes of CTL exposure to the bilayers, microclusters containing activated Src kinases were seen in the cSMAC and the pSMAC of $CD8^+$ CTL, while $CD4^+$ CTL exhibited the activated Src containing microclusters mostly in the pSMAC (Fig. 2A,C,D). Similar staining patterns were observed after 10 minutes of CTL contact with the bilayers (Fig. S6). Although the number of clusters per cell at the same pMHC density on the bilayers was similar, the integrated fluorescence intensity per cluster, which reflects the number of activated Src kinases, was higher in $CD8^+$ CTL than in $CD4^+$ CTL (Fig. 2E,F). We then compared the location and the number of activated Src kinases per cluster at contact surface of the same $CD8^+$ CTL stimulated with strong agonist peptide loaded onto either intact or mutated HLA-A2(A245V). $CD8^+$ CTL exposed to the bilayers containing pHLA-A2(A245V) resulted in a lower number of activated Src kinases per cluster and their disappearance from the cSMAC (Fig. 2B,D,E,F and Fig. S6). We also compared the amount of activated Src per cluster in 68A62 $CD8^+$ CTL stimulated with either strong (IV9-HLA-A2) or weak (IV9-A7-HLA-A2) agonists. Even though we utilized a higher density of weak agonist on bilayers, we found a greater amount of activated Src per cluster in $CD8^+$ CTL exposed to bilayers containing strong agonist (Fig. S7). Since the size of the microclusters does not depend on the density of cognate pMHC (Varma et al., 2006), these data provide evidence that stronger TCR stimulation leads to faster accumulation of activated Src kinases at the interface.

Overall, these data suggest that the kinetics of early TCR signaling rather than the maximal intensity of signaling at later times determines the different patterns of granule polarization observed during more and less effective cytolytic responses.

Pattern of granule polarization depends on the kinetics of early TCR signaling

To establish a link between the kinetics of early TCR signaling and the pattern of granule polarization, we first analyzed the dependence of early signaling kinetics on the strength of TCR stimulation. For this purpose we utilized QD bearing pMHC ligands that engage TCR with different strengths, namely, MHC loaded with strong (IV9-HLA-A2) or weak (IV9-A7-HLA-A2) agonist peptides recognized by 68A62 $CD8^+$ CTL, IV9-HLA-A2(A245V) agonist with a mutation in HLA-A2 that abrogates HLA-A2-CD8 interactions, and agonist PP16-HLA-DR1 that stimulates $CD4^+$ CTL (Fig. S8). We then measured the kinetics of intracellular Ca^{2+} accumulation induced by these QD/pMHC conjugates as an indicator of early TCR signaling (Anikeeva et al., 2006).

CER43 $CD8^+$ CTL TCR engagement by QD/GL9-HLA-A2 led to a rapid and robust Ca^{2+} response even when the concentration of QD/GL9-HLA-A2 was decreased to 1 nM (Fig. 3A, top). In contrast, cognate QD/PP16-HLA-DR1 failed to induce Ca^{2+} mobilization in less effective AC25 $CD4^+$ CTL unless a higher concentration (100 nM) of QD/PP16-HLA-DR1 was used (Fig. 3A, bottom). Moreover, while Ca^{2+} mobilization in $CD8^+$ CTL can be readily measured in the absence of Ca^{2+} in the extracellular medium (Fig. S9B), binding of QD/PP16-HLA-DR1 to $CD4^+$ CTL under these conditions induced a barely detectable increase in the level of intracellular Ca^{2+} even at a high concentration of larger QD/PP16-HLA-DR1 conjugates (Fig. S9C). Nevertheless, the $CD4^+$ CTL could mount a strong Ca^{2+} response induced by TCR cross-linking with anti-CD3 antibodies that was very similar to that observed for $CD8^+$ CTL (Fig. S9A) showing no intrinsic defect in the ability of $CD4^+$ CTL to mobilize Ca^{2+}.

Additional evidence demonstrating a link between the kinetics of early TCR signaling and the pattern of granule polarization was provided by experiments in which we altered the strength of TCR stimulation of the same $CD8^+$ CTL clone by weakening either the TCR-pMHC-I or CD8-MHC-I interactions and consequently the kinetics of early signaling. Stimulation of 68A62 $CD8^+$ CTL with weak agonist QD/IV9-A7-HLA-A2 resulted in slower signaling

kinetics and lower magnitude of the response (Fig. 3B). Binding of QD bearing mutated HLA-A2(A245V) loaded with strong agonist IV9 to 68A62 $CD8^+$ CTL led to slower signaling and a decreased magnitude of the response as well (Fig. S9D).

Antigen-independent variations in intracellular Ca^{2+} flux alter the pattern of polarized granules in cytolytic synapses

To determine whether variations in the concentration of intracellular Ca^{2+} initiate signaling that dictates the observed differences in granule polarization pattern, we utilized pharmacological agents to vary the intracellular level of Ca^{2+} in CTL stimulated with either strong or weak agonist ligands.

Figure 4A shows that $CD8^+$ CTL treatment with the calcium chelator BAPTA delayed the kinetics of Ca^{2+} accumulation induced by cognate QD/pMHC-I ligands in a dose-dependent manner, while the maximum level of Ca^{2+} flux was not altered at BAPTA concentration up to 10 μM. In contrast, treatment of $CD8^+$ CTL with various concentrations of calcium ionophore ionomycin resulted in a very swift and dose dependent increase in intracellular Ca^{2+} (Fig. 4B). The Ca^{2+} rise was so rapid that it was impossible to measure the time required to reach the maximum level at each concentration. Consistent with these data, BAPTA treated $CD8^+$ CTL exposed to ICAM-1 lipid bilayers containing strong agonist pHLA-A2 led to the dispersion of granules to the periphery such that most of the granules were observed in the pSMAC of the synapses (Fig. 4C and Fig. S10). Treatment of CTL with weak agonist pMHC plus ionomycin at 1 μM resulted in an opposite effect that promoted granule redistribution to the cSMAC of the synapse (Fig. 4D and Fig. S11).

These data show that rapid Ca^{2+} flux kinetics result in a central granule location, while slow Ca^{2+} kinetics alter the granule positioning to the periphery.

The two principal granule movements can be uncoupled

Since granule movements along the microtubules can occur much faster than MTOC polarization (Huse et al., 2007; Kuhne et al., 2003; Poenie et al., 1987; Ross et al., 2006), the above data suggest that the kinetics of downstream Ca^{2+} signaling could function as a temporal regulator of the two principal granule movements. To provide evidence for such regulation we sought to uncouple these two movements.

MTOC polarization to the mature synapse requires the tethering of microtubules to remodeled actin cytoskeleton, while granule concentration around the MTOC can occur without cytoskeleton remodeling and mature synapse formation (Stinchcombe et al., 2006). Therefore, to disable MTOC polarization we utilized a glass-supported bilayer system that permits the exclusion of cellular adhesion and actin cytoskeleton remodeling. We stimulated $CD8^+$ and $CD4^+$ CTL with a high concentration of agonist pMHC ligands incorporated into lipid bilayers devoid of adhesion molecules and found that TCR-pMHC interactions mediate CTL attachment to the bilayer surface through the formation of a thin stalk-like structure as previously described (Anikeeva et al., 2005). TCR stimulation with agonist pMHC alone induced lytic granule clustering around the MTOC of both $CD4^+$ and $CD8^+$ CTL (Fig. 5A, top). Importantly, granule accumulation around the MTOC was observed in the absence of MTOC translocation to the bilayers, as was evident from the staining of the Golgi complex whose intracellular location overlaps with the MTOC (Geiger et al., 1982; Kupfer et al., 1983)(Fig. 5A). CTL exposure to non-cognate pMHC did not lead to granule concentration near the MTOC (Fig. 5A, bottom). Thus, TCR signaling alone can induce granule movement along microtubules towards the MTOC without the MTOC polarization in both CTL.

We next wanted to demonstrate that variations in the temporal regulation of the two movements could change the pattern of granule polarization at the synapse. If the granules assume the central location only when they are recruited to the MTOC prior to but not after MTOC polarization, increase in the strength of TCR stimulation after MTOC polarization and synapse formation should not suffice to deliver the granules to the cSMAC. To test this assumption we first exposed $CD8^+$ CTL to bilayers containing a weak agonist pMHC-I ligand and ICAM-1, a condition that causes the granules to be polarized to the pSMAC (Fig. 5B, left panel). We then added fluorescent-labeled His-tagged strong pMHC-I agonist to the bilayer, which is known to induce rapid early TCR signaling (Fig. 3B, top) causing granule polarization to the cSMAC (Fig. 1A, left). As expected, the strong agoinst pMHC-I was observed in the cSMAC, but granules still remained in the pSMAC (Fig. 5B, middle). In control experiments, sequential immobilization of weak and then strong agonist ligands on the bilayer prior to CTL exposure resulted in the typical granule polarization pattern observed for $CD8^+$ CTL stimulated with strong agonist ligand (Fig. 5B, right). These data show that the induction of strong TCR stimulation after the formation of the mature cytolytic synapse and MTOC polarization precludes granules reaching the MTOC. Thus, weakening the initial TCR stimulation in $CD8^+$ CTL results in a detour of the granules through the pSMAC, similar to that observed in less effective $CD4^+$ CTL.

Granules are delivered to the secretory domain with different kinetics

Using TIRF microscopy, we monitored the dynamics of granule release by the appearance of a secretory lysosomal membrane protein CD107a on the contact surface of CTL exposed to bilayers containing cognate pMHC-I and ICAM-1 (Beal et al., 2008). The release of cytolytic granules was detected in the cSMAC of the cytolytic synapses of both $CD8^+$ and $CD4^+$ CTL (Fig. 6A). Thus, CTL release granules through a secretory domain within the cSMAC (Stinchcombe et al., 2001) regardless of their effectiveness. The CD107a staining did not emerge gradually over the entire cSMAC, but initially appeared as one to a few micron-scale spots in the center of the cSMAC or near the cSMAC/pSMAC boundary (see Movies). This staining pattern reflected membrane fusion events between secretory lysosomes and the plasma membrane. CD107a did not diffuse away from these sites, but remained in place as additional exocytic events took place filling much of the cSMAC with CD107a puncta. This behavior allows us to follow the kinetics of granule release over the first few minutes of cytolytic synapse formation (Fig. 6A and Fig. S12). CD107a staining in the $CD8^+$ CTL secretory domain was detectable by 1 min while the staining in the $CD4^+$ CTL secretory domains was not observed until 3 min after the CTL contacted the bilayers (Fig. 6A). In accord with this observation, the frequency of $CD4^+$ CTL in which degranulation was evident was significantly lower than that of $CD8^+$ CTL at early time points (Fig. 6B). At high density of cognate pMHC in the bilayers, a statistically significant difference in the percentage of the degranulated CTL was observed for the first 3 minutes, while this difference persisted for up to 5 minutes at low epitope density (Fig. 6B). Thus, it initially takes a longer time for $CD4^+$ CTL to deliver the granules to the secretory domain. Degranulation by $CD8^+$ CTL was slower when CD8-MHC-I interactions were abrogated (Fig. S13) and was similar to that observed for $CD4^+$ CTL (Fig. 6).

These data suggest that the dynamics of CTL degranulation is associated with the pattern of granule polarization and is governed by the kinetics of early TCR signaling.

DISCUSSION

Previous studies have defined two principal movements involved in cytolytic granule polarization, namely, granule recruitment to the MTOC and MTOC polarization to the CTL contact interface. While both movements require productive TCR engagement (Poenie et al., 2004; Stinchcombe et al., 2006), how TCR signaling coordinates these movements has not

been established. We have shown that variations in the kinetics of early TCR signaling determine the difference in temporal and spatial coordination of the two principal movements. This accounts for two distinct pathways of granule delivery that are characterized by divergent patterns of granule polarization at the CTL contact interface (Fig. 7). The two pathways are not mutually exclusive and can operate in a single CTL at the same time regardless of T cell lineage.

Both principal movements require the activation of a similar set of signaling proteins induced by TCR engagement. LAT is recruited to the cell membrane and subsequently PLCγ is activated, which cleaves PIP_2 and produces DAG and IP_3; the latter initiates mobilization of intracellular Ca^{2+} (Huse et al., 2008; Stinchcombe and Griffiths, 2007)(**see** Fig. 7). DAG has recently been shown to mediate MTOC translocation in T cells that is Ca^{2+}-independent (Quann et al., 2009). At the same time, our data provide evidence that granule movement towards the MTOC is regulated by the kinetics of intracellular Ca^{2+} accumulation (Figs. 3, 4 and 5). This is in accord with the analysis of granule movement in another system showing that a rise in intracellular Ca^{2+} concentration increases the dynein mediated aggregation velocity of pigment granules by 4.4 fold (Ribeiro and McNamara, 2007). Thus, granule concentration around the MTOC and MTOC polarization appear to be independently regulated by Ca^{2+} mediated signaling and DAG-dependent signaling (Fig. 7). Such a signaling dichotomy supports the proposed mechanism controlling the two different paths of granule delivery to the secretory domain. Indeed, variations in the kinetics of Ca^{2+} signaling determine whether granules are recruited to the MTOC prior to MTOC polarization and delivered via the short path or whether granule movement to the MTOC is delayed and they are diverted to a longer path. The longer path takes granules to the periphery of the synapse and then moves them tangentially across the pSMAC to fuse at the outer edge of the secretory domain.

Although granules can be delivered via short and long pathways, granule release occurs within the cSMAC (**see** Fig. 6). The cSMAC membrane, which is deprived of an underlying actin cytoskeletal network, seems to be very well suited for efficient membrane fusion, mediating rapid endocytosis and exocytosis. Most likely, vesicle docking, priming, and membrane fusion, which are required for granule release, are mediated by specialized proteins, which can operate only in a particular membrane environment termed “active zones” (Spiliotis and Nelson, 2003).

How does Ca^{2+} regulate dynein dependent granule movement from the “plus” end to the “minus” end of microtubules? Since dynein motors can function in the absence of Ca^{2+} in a cell free system (Gennerich et al., 2007), Ca^{2+} exercises its activity indirectly through downstream events. The nature of these events is not known at present and remains to be understood.

Initial translocation of the MTOC appears to be DAG mediated and Ca^{2+}-independent (Quann et al., 2009). On the other hand, MTOC polarization to the mature synapse is associated with F-actin remodeling and segregation. It is thought that upon segregation F-actin pulls the attached microtubules to the periphery of the synapse (Stinchcombe and Griffiths, 2007). Consistent with this, ADAP-associated dynein motors have been located at the periphery of the pSMAC and reel in the attached microtubules, forcing the MTOC to polarize to the synapse (Combs et al., 2006). In addition, the exposure of $CD8^+$ CTL to lipid bilayers containing only cognate pMHC proteins resulted in the formation of a small contact area and partial translocation but not complete MTOC polarization towards the CTL/bilayer interface (Anikeeva et al., 2005). We would like to propose that while initial MTOC translocation of the MTOC toward the CTL contact area is regulated by DAG-dependent signaling (Quann et al., 2009), complete MTOC polarization to the mature synapse, which is characterized by

juxtaposition of the centrioles and the contact CTL membrane (Stinchcombe et al., 2006), requires F-actin remodeling and actin ring formation (Combs et al., 2006)(**see** Fig. 7).

Our data show that the kinetics but not the magnitude of TCR signaling determines the principal difference between the two pathways of granule delivery, which is manifested in the distinct patterns of granule polarization. We have found that each microcluster formed upon effective CTL stimulation contains a larger amount of activated Src molecules (Fig. 2) resulting in faster accumulation of activated signaling proteins and Ca^{2+} in the cytoplasm of these CTL during early signaling (Fig. 3). Later, however, when full-blown signaling is developed, there is virtually no difference in the magnitude of intracellular signaling in more or less effective CTL, as was evident from the level of intracellular Ca^{2+} (Fig. S5). Not surprising is that the integrated amount of activated Scr kinases at the interface was only slightly higher in CTL undergoing more effective stimulation and the difference was not statistically significant (data not shown).

Activated Src kinases reflecting TCR-mediated membrane proximal signaling were observed in the cSMAC of $CD8^+$ CTL but not of $CD4^+$ CTL (Fig. 2A,C,D). The absence of cSMAC signaling in $CD4^+$ CTL is in line with previous studies highlighting the role of the cSMAC in down regulation of signaling in $CD4^+$ T cells (Lee et al., 2002; Varma et al., 2006; Yokosuka et al., 2005). The proximal signaling in the cSMAC of $CD8^+$ CTL indicates that perhaps signaling can persist in the cSMAC with strong TCR stimulation. This finding raises a question whether all strong signals are necessarily turned off in the cSMAC. Recently, it has been shown that exposure of $CD4^+$ T cells to bilayers with a lower density of cognate pMHC that induce relatively weak TCR-mediated signaling results in the appearance of activated signaling proteins in the cSMAC at a later time point (Cemerski et al., 2007). Most likely, this late signaling is not associated with the rapid release of cytolytic granules that occurs within minutes after antigen recognition and does not require the expression of new genes or de novo protein synthesis (Sykulev et al., 1996). Persistence of a very strong TCR signal may induce apoptosis and is unlikely associated with T cell proliferation.

The magnitude of full-blown signaling during more and less effective cytolytic responses was very similar (Fig. S4) leading to a practically identical amount of released granules (Beal et al., 2008). However, analysis of the kinetics of granule release showed a significant delay in degranulation by CTL that exercise a less effective cytolytic response (Fig. 6). The ability to rapidly concentrate granules around the MTOC seems to endow CTL with the capacity to exercise a more effective cytolytic response against the next target cells it attacks. When a CTL leaves a target cell, often the granules remain concentrated around the MTOC even though the MTOC moves away from the contact area (Stinchcombe and Griffiths, 2007). This allows CTL to more rapidly release granules towards the next target cell. This is reminiscent of the “primed state” of the highly cytotoxic NK cell line KHYG-1 that contains lytic granules constitutively clustered around the MTOC (Suck et al., 2006). The central granule location and rapid granule release appear to be instrumental for the ability of CTL to kill a greater number of the infected cells within a limited time when the CTL are outnumbered (Supplemental Data).

We have previously shown that the formation of a stable pSMAC confines released granules at the CTL/target cell interface, increasing the ability to kill target cells with a minimal amount of granules (Beal et al., 2008). On the other hand, the actin ring of the peripheral junction serves to recruit dynein in an ADAP-dependent manner to the synapse, which is essential for MTOC polarization to the mature synapse ensuring efficient granule delivery to the secretory domain (Combs et al., 2006; Stinchcombe et al., 2006). Thus, the formation of the pSMAC serves two different purposes during the CTL response, with both facilitating the effectiveness of cytolytic response, but in entirely different ways. It appears, therefore, that the same molecular hardware in a cell can be utilized for various needs.

EXPERIMENTAL PROCEDURES

Cells

The human flu-specific $CD8^+$ CTL clone CER43 that recognizes the matrix protein peptide GILGFVFTL (GL9)(Gotch et al., 1987) was kindly provided by Antonio Lanzavecchia and human $CD8^+$ CTL clone 68A62 that recognizes the ILKEPVHGV (IV9) peptide from HIV reverse transcriptase was a gift from Bruce D. Walker. The human HIV-specific $CD4^+$ CTL clone AC-25 that recognizes PEVIPMFSALSEGATP (PP16) peptide from HIV Gag protein was derived as described (Norris et al., 2001). The T2 ($HLA\text{-}A2^+$) lymphoblast cell line transfected with HLA-DRB1*0101 (DRB1), designated T2-DR1, was kindly provided by Lisa Denzin.

Proteins and peptides

Soluble His_6-tagged HLA-DRB1 as well as HLA-A2 intact and mutated (A245V) molecules were produced and purified as previously described (Beal et al., 2008).

Peptide PP16 (Norris et al., 2001) was synthesized by BioSynthesis. Control peptides SDWRFLRGYHQYA (A2) from HLA-A2 and RVEYHFLSPYVSPKESP (TfR) from transferrin receptor, which interact with HLA-DRB1, were kindly provided by Larry Stern (Chicz et al., 1992). Research Genetics synthesized GL9 peptide. The peptide IV9 (Tsomides et al., 1991) and its variants with Alanine substitutions at the P7 and P4 positions (IV9-A7 and IV9-A4) were a gift from Herman N. Eisen.

Antibodies

Hybridoma OKT 3 producing antibodies to CD3 was purchased from ATCC. Monovalent Fab fragments of anti-CD107a antibody were produced and labeled with Alexa Fluor 568 as described (Beal et al., 2008). Rabbit polyclonal antibody specific for phospho-Src family kinases (Tyr416) was purchased from Cell Signaling Technology. Alexa Fluor 546 goat anti-rabbit IgG $F(ab')_2$ were obtained from Invitrogen.

QD preparation

The DHLA-capped QD-520 and QD-620 (emission wavelength 520 or 620 nm, respectively) were produced as previously described (Anikeeva et al., 2006; Anikeeva et al., 2009). For some experiments we utilized QDs encapsulated into lipid micelles (Evident Technology) as described elsewhere (Anikeeva et al., 2009).

Ca^{2+} Flux Measurements

CTL were loaded for 30 min at 37°C with either 5 μM Fura Red AM or 2 μM Fluo-3 (Invitrogen) as described (Anikeeva et al., 2006). Freshly prepared QD/pMHC conjugates were added at various concentrations (as designated) to CTL suspension in the assay buffer (Dulbecco's PBS containing 1 mM $CaCl_2$, 0.1 mM $MgCl_2$, 5 mM glucose, and 0.025% BSA), and the samples were analyzed by flow cytometry. Data collection was initiated about 20 s after the QD/pMHC conjugates were combined with the CTL following background measurements. The data were evaluated using FlowJo software (Tree Star).

CTL treatment with BAPTA and ionomycin

BAPTA/AM (Calbiochem) was added to CTL at various concentrations, and the CTL were incubated for 20 min at 37°C. In some experiments the LysoTracker red (see below) or Fluo-3 was added after BAPTA loading. After washing the CTL were resuspended in appropriate medium and used for Ca^{2+} measurements or injected into the planar bilayer (see below). Ionomycin was added to CTL suspension at various concentrations and Ca^{2+} flux was

immediately measured in Fluo-3 labeled CTL by flow cytometry. In some experiments, CTL were first adhered to ICAM-1 bilayers and then were treated with a mixture of IV9-A7-HLA-A2 weak agonist plus ionomycin (1 μM).

Planar lipid bilayers and confocal microscopy

Planar lipid bilayers were prepared as previously described (Anikeeva et al., 2005; Grakoui et al., 1999; Somersalo et al., 2004). Cy5-ICAM-1-GPI or Cy5-ICAM-1-His were incorporated into the bilayers at 200–300 molecules/μm^2. His_6-tagged pMHC complexes (either unlabeled or labeled with Alexa Fluor 488) were incorporated into the bilayers 500 molecules/μm^2. In some experiments the density of pMHC on bilayer was varied as indicated. For some experiments liposomes that contained biotinyl CAP functionalized lipid (Avanti Polar Lipids) at 0.01 mol% were used to prepare bilayers. Streptavidin (4 μg/ml) and monobiotinylated anti-CD3 (OKT 3) monoclonal antibody (2 μg/ml) were reacted sequentially with the biotinylated bilayers. CTL were injected into pre-warmed to 37°C flow cells. In some experiments CTL were labeled with Bodipy NBD C_6 ceramide (Invitrogen) and/or LysoTracker Red DND-99 (Invitrogen). The cells were imaged on a confocal fluorescence microscope (Zeiss LSM510) or an IX-70 Olympus inverted microscope.

TIRF imaging

TIRF imaging of CTL degranulation on the bilayer was assessed using Alexa Fluor 586-labeled Fab fragments of anti-CD107a (LAMP-1) antibody (Betts et al., 2003) as previously described (Beal et al., 2008). To image activated Src kinases, CTL attached to the bilayers were fixed with 2% paraformaldehyde, permeabilized with 0.1% Triton X-100 and stained for phospho-Src kinases. All TIRF imaging was performed on an Olympus inverted IX-70 microscope using the 60×1.45 N.A. TIRF objective from Olympus.

Image Analysis

To determine granule localization at the bilayer interface with regards to the domains of the IS, regions were drawn around the areas corresponding to the pSMAC and cSMAC. The percentage of stained cytolytic granules in the pSMAC and the cSMAC was calculated by quantifying groups of bright pixels in each domain. Groups of bright pixels that overlapped with the region lines drawn to separate the pSMAC and cSMAC areas were scored into the region designated as pSMAC/cSMAC junction.

To evaluate the amount of activated Src kinases within pSMAC or cSMAC of the IS, regions were drawn around both domains. Local background had been subtracted using Image J. The integrated intensity for each pSMAC and cSMAC region was measured with MetaMorph and the percentage of phospho-Src signal that is present in each domain of the IS was calculated. We further evaluated the amount of the signaling clusters and integrated fluorescence intensity of each signaling cluster using the Integrated Morphometry Analysis (IMA) function of MetaMorph. The average of the integrated fluorescence of the signaling clusters for each cell was calculated and expressed in arbitrary units.

CTL-target cell conjugation and immunofluorescence analysis of granule distribution

T2.DR1 target cells were loaded with 10^{-5}M concentration of cognate peptide (either IV9 or PP16) and were mixed with corresponding CTL at a 1:1 ratio as described (Cannon et al., 2001). Cells were then gently pipetted onto poly-L-lysine coated coverslips and fixed with methanol. To visualize actin and cytolytic granules, rabbit polyclonal antibody against actin (Sigma) and anti-perforin monoclonal antibody (clone dG9, Biolegend) were used, respectively (Stinchcombe et al., 2001). Coverslips were mounted using ProLong Gold

(Invitrogen). Samples were examined using a Zeiss LSM 510 META Confocal microscope. Data were analyzed with Slidebook v4.0 software (3I).

Supplementary Material

Refer to Web version on PubMed Central for supplementary material.

Acknowledgments

This work was supported by NIH grants to Y.S. (AI52812), M.L.D (AI44931; AI52812) and P.J.N (AI067854). We thank Alexandra Zanin-Zhorov for purification of His_6-tagged ICAM-1 and Tatiana Mareeva for help with production and purification of anti-CD107 Fab fragments. We also thank Santosh Vardhana for help with TIRF imaging, the Burkhardt lab for help with conjugate imaging and the Kimmel Cancer Institute Bioimaging facility where some experiments were performed. John Heitman is acknowledged for the advice regarding the $CD4^+$ CTL maintenance. We thank Art Weiss for suggesting the use of anti-CD3 antibodies as a generic strong TCR stimulus. A.M.B. was supported in part by NRSA training grant T32-CA 0983.

References

Anikeeva N, Lebedeva T, Clapp AR, Goldman ER, Dustin ML, Mattoussi H, Sykulev Y. Quantum dot/peptide-MHC biosensors reveal strong CD8-dependent cooperation between self and viral antigens that augment the T cell response. Proc Natl Acad Sci U S A 2006;103:16846–16851. [PubMed: 17077145]

Anikeeva N, Mareeva T, Liu W, Sykulev Y. Can oligomeric T-cell receptor be used as a tool to detect viral peptide epitopes on infected cells? Clin Immunol 2009;130:98–109. [PubMed: 18845488]

Anikeeva N, Somersalo K, Sims TN, Thomas VK, Dustin ML, Sykulev Y. Distinct role of lymphocyte function-associated antigen-1 in mediating effective cytolytic activity by cytotoxic T lymphocytes. Proc Natl Acad Sci U S A 2005;102:6437–6442. [PubMed: 15851656]

Appay V, Zaunders JJ, Papagno L, Sutton J, Jaramillo A, Waters A, Easterbrook P, Grey P, Smith D, McMichael AJ, et al. Characterization of CD4(+) CTLs ex vivo. J Immunol 2002;168:5954–5958. [PubMed: 12023402]

Beal AM, Anikeeva N, Varma R, Cameron TO, Norris PJ, Dustin ML, Sykulev Y. Protein kinase Ctheta regulates stability of the peripheral adhesion ring junction and contributes to the sensitivity of target cell lysis by CTL. J Immunol 2008;181:4815–4824. [PubMed: 18802085]

Betts MR, Brenchley JM, Price DA, De Rosa SC, Douek DC, Roederer M, Koup RA. Sensitive and viable identification of antigen-specific CD8+ T cells by a flow cytometric assay for degranulation. J Immunol Methods 2003;281:65–78. [PubMed: 14580882]

Brander C, Frahm N, Walker BD. The challenges of host and viral diversity in HIV vaccine design. Curr Opin Immunol 2006;18:430–437. [PubMed: 16777397]

Cannon JL, Labno CM, Bosco G, Seth A, McGavin MH, Siminovitch KA, Rosen MK, Burkhardt JK. Wasp recruitment to the T cell:APC contact site occurs independently of Cdc42 activation. Immunity 2001;15:249–259. [PubMed: 11520460]

Cemerski S, Das J, Locasale J, Arnold P, Giurisato E, Markiewicz MA, Fremont D, Allen PM, Chakraborty AK, Shaw AS. The stimulatory potency of T cell antigens is influenced by the formation of the immunological synapse. Immunity 2007;26:345–355. [PubMed: 17346997]

Chicz RM, Urban RG, Lane WS, Gorga JC, Stern LJ, Vignali DAA, Strominger JL. Predominant naturally processed peptides bound to HLA-DR1 are derived from MHC-related molecules and are heterogeneous in size. Nature 1992;358:764–768. [PubMed: 1380674]

Combs J, Kim SJ, Tan S, Ligon LA, Holzbaur EL, Kuhn J, Poenie M. Recruitment of dynein to the Jurkat immunological synapse. Proc Natl Acad Sci U S A 2006;103:14883–14888. [PubMed: 16990435]

Gao GF, Jakobsen BK. Molecular interactions of coreceptor CD8 and MHC class I: the molecular basis for functional coordination with the T-cell receptor. Immunol Today 2000;21:630–636. [PubMed: 11114424]

Geiger B, Rosen D, Berke G. Spatial relationships of microtubule-organizing centers and the contact area of cytotoxic T lymphocytes and target cells. J Cell Biol 1982;95:137–143. [PubMed: 6982900]

Gennerich A, Carter AP, Reck-Peterson SL, Vale RD. Force-induced bidirectional stepping of cytoplasmic dynein. Cell 2007;131:952–965. [PubMed: 18045537]

Gotch F, Rothbard J, Howland K, Townsend A, McMichael A. Cytotoxic T lymphocytes recognize a fragment of influenza virus matrix protein in association with HLA-A2. Nature 1987;326:881–882. [PubMed: 2437457]

Grakoui A, Bromley SK, Sumen C, Davis MM, Shaw AS, Allen PM, Dustin ML. The immunological synapse: a molecular machine controlling T cell activation. Science 1999;285:221–227. [PubMed: 10398592]

Hahn S, Gehri R, Erb P. Mechanism and biological significance of CD4-mediated cytotoxicity. Immunol Rev 1995;146:57–79. [PubMed: 7493761]

Heller KN, Gurer C, Munz C. Virus-specific CD4+ T cells: ready for direct attack. J Exp Med 2006;203:805–808. [PubMed: 16549599]

Huse M, Klein LO, Girvin AT, Faraj JM, Li QJ, Kuhns MS, Davis MM. Spatial and temporal dynamics of T cell receptor signaling with a photoactivatable agonist. Immunity 2007;27:76–88. [PubMed: 17629516]

Huse M, Quann EJ, Davis MM. Shouts, whispers and the kiss of death: directional secretion in T cells. Nat Immunol 2008;9:1105–1111. [PubMed: 18800163]

Kuhne MR, Lin J, Yablonski D, Mollenauer MN, Ehrlich LI, Huppa J, Davis MM, Weiss A. Linker for activation of T cells, zeta-associated protein-70, and Src homology 2 domain-containing leukocyte protein-76 are required for TCR-induced microtubule-organizing center polarization. J Immunol 2003;171:860–866. [PubMed: 12847255]

Kupfer A, Dennert G, Singer SJ. Polarization of the Golgi apparatus and the microtubule-organizing center within cloned natural killer cells bound to their targets. Proc Natl Acad Sci U S A 1983;80:7224–7228. [PubMed: 6359165]

Lee K, Holdorf A, Dustin ML, Chan AC, Allen PA, Shaw AS. Tyrosine kinase activation precedes formation of the immunological synapse. Science 2002;295:1539–42. [PubMed: 11859198]

McMichael AJ. HIV vaccines. Annu Rev Immunol 2006;24:227–255. [PubMed: 16551249]

Monks C, Freiberg B, Kupfer H, Sciaky N, Kupfer A. Three-dimensional segregation of supramolecular activation clusters in T cells. Nature 1998;395:82–86. [PubMed: 9738502]

Norris PJ, Sumaroka M, Brander C, Moffett HF, Boswell SL, Nguyen T, Sykulev Y, Walker BD, Rosenberg ES. Multiple effector functions mediated by human immunodeficiency virus-specific CD4(+) T-cell clones. J Virol 2001;75:9771–9779. [PubMed: 11559810]

Pasternack MS, Verret CR, Liu MA, Eisen HN. Serine esterase in cytolytic T lymphocytes. Nature 1986;322:740–743. [PubMed: 3489187]

Poenie M, Kuhn J, Combs J. Real-time visualization of the cytoskeleton and effector functions in T cells. Curr Opin Immunol 2004;16:428–438. [PubMed: 15245735]

Poenie M, Tsien RY, Schmitt-Verhulst A-M. Sequential activation and lethal hit measured by [Ca^{2+}] in individual cytolytic T cells and targets. EMBO J 1987;6:2223–2232. [PubMed: 3499312]

Potter TA, Grebe K, Freiberg B, Kupfer A. Formation of supramolecular activation clusters on fresh ex vivo CD8+ T cells after engagement of the T cell antigen receptor and CD8 by antigen-presenting cells. Proc Natl Acad Sci U S A 2001;98:12624–12629. [PubMed: 11606747]

Quann EJ, Merino E, Furuta T, Huse M. Localized diacylglycerol drives the polarization of the microtubule-organizing center in T cells. Nat Immunol 2009:627–635. [PubMed: 19430478]

Ribeiro M, McNamara JC. Calcium movements during pigment aggregation in freshwater shrimp chromatophores. Pigment Cell Res 2007;20:70–77. [PubMed: 17250550]

Ross JL, Wallace K, Shuman H, Goldman YE, Holzbaur EL. Processive bidirectional motion of dynein-dynactin complexes in vitro. Nat Cell Biol 2006;8:562–570. [PubMed: 16715075]

Somersalo K, Anikeeva N, Sims TN, Thomas VK, Strong RK, Spies T, Lebedeva T, Sykulev Y, Dustin ML. Cytotoxic T lymphocytes form an antigen-independent ring junction. J Clin Invest 2004;113:49–57. [PubMed: 14702108]

Spiliotis ET, Nelson WJ. Spatial control of exocytosis. Curr Opin Cell Biol 2003;15:430–437. [PubMed: 12892783]

Stinchcombe JC, Bossi G, Booth S, Griffiths GM. The Immunological Synapse of CTL Contains a Secretory Domain and Membrane Bridges. Immunity 2001;15:751–761. [PubMed: 11728337]

Stinchcombe JC, Griffiths GM. Secretory mechanisms in cell-mediated cytotoxicity. Annu Rev Cell Dev Biol 2007;23:495–517. [PubMed: 17506701]

Stinchcombe JC, Majorovits E, Bossi G, Fuller S, Griffiths GM. Centrosome polarization delivers secretory granules to the immunological synapse. Nature 2006;443:462–465. [PubMed: 17006514]

Suck G, Branch DR, Aravena P, Mathieson M, Helke S, Keating A. Constitutively polarized granules prime KHYG-1 NK cells. Int Immunol 2006;18:1347–1354. [PubMed: 16849396]

Sykulev Y, Joo M, Vturina I, Tsomides TJ, Eisen HN. Evidence that a single peptide-MHC complex on a target cell can elicit a cytolytic T cell response. Immunity 1996;4:565–571. [PubMed: 8673703]

Tsomides TJ, Walker BD, Eisen HN. An optimal viral peptide recognized by $CD8^+$ T cells binds very tightly to the restricting class I major histocompatibility complex protein on intact cells but not to the purified class I protein. Proc. Natl. Acad. Sci. USA 1991;88:11276–11280.

Varma R, Campi G, Yokosuka T, Saito T, Dustin ML. T cell receptor-proximal signals are sustained in peripheral microclusters and terminated in the central supramolecular activation cluster. Immunity 2006;25:117–127. [PubMed: 16860761]

Werlen G, Palmer E. The T-cell receptor signalosome: a dynamic structure with expanding complexity. Curr Opin Immunol 2002;14:299–305. [PubMed: 11973126]

Yokosuka T, Sakata-Sogawa K, Kobayashi W, Hiroshima M, Hashimoto-Tane A, Tokunaga M, Dustin ML, Saito T. Newly generated T cell receptor microclusters initiate and sustain T cell activation by recruitment of Zap70 and SLP-76. Nat Immunol 2005;6:1253–1262. [PubMed: 16273097]

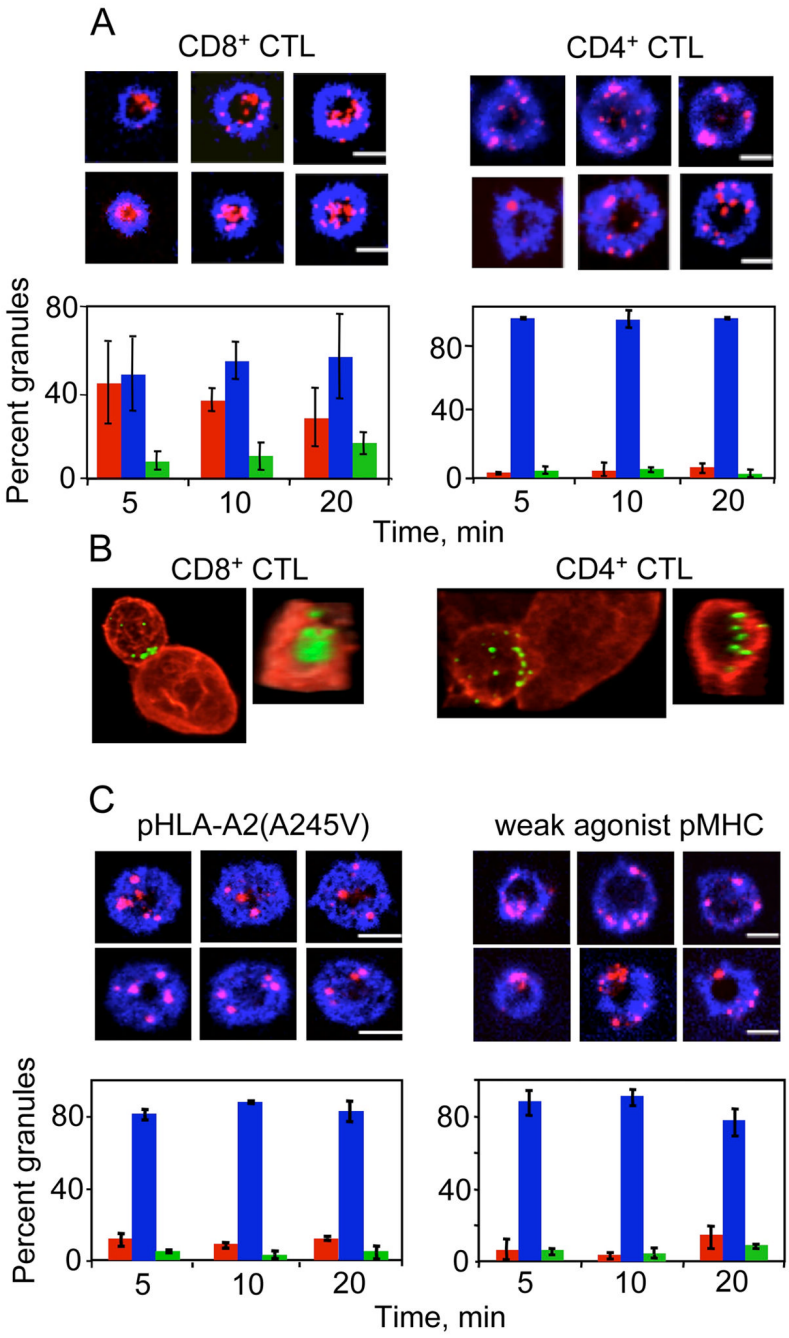

Figure 1. Integrated strength of TCR engagement influences the pattern of granule polarization within the cytolytic synapse

(**A**) $CD8^+$ CTL concentrate a significant amount of polarized granules in the cSMAC, while polarized granules in $CD4^+$ CTL are mostly observed within the pSMAC. Representative images of $CD8^+$ CER43 CTL (top left) and $CD4^+$ AC-25 CTL (top right) interacting with bilayers containing respective agonist pMHC ligands and ICAM-1 are shown. ICAM-1 is blue and granule staining is red. Scale bar: 5μm. The percent of granules localized in the cSMAC (red bars), pSMAC (blue bars), and cSMAC/pSMAC junction (green bars) in $CD8^+$ CTL (bottom left) and $CD4^+$ CTL (bottom right) at the CTL/bilayer interface is shown in the graphs. More than 43 IS forming cells were analyzed for each time point in 3 independent experiments.

(B). Distribution of polarize granules in $CD8^+$ (left) and $CD4^+$ (right) CTL contacting live target cells bearing respective cognate pMHC proteins. One representative conjugate from two independent experiments, each from $CD8^+$ CTL and $CD4^+$ CTL, is shown (left panels). Corresponding *en face* projections of the cell-cell contact site are presented on the right panels. 82.4% (14 out of 17) of the $CD8^+$ CTL conjugates had granules (green) within the cSMAC surrounded by a peripheral actin ring (red). The majority (82.6% or 14 out of 18) of the $CD4^+$ CTL conjugates demonstrated scattered granules at the synapse.

(C) Weakening of TCR-pMHC interactions in $CD8^+$ CTL resulted in redistribution of polarized granules to the pSMAC. Top: Representative images of $CD8^+$ CTL interacting with bilayers containing ICAM-1 and the indicated pMHC molecules are shown. ICAM-1 is in blue and granules are in red. Scale bar: 5μm. Bottom: The percentage of granules localized in the pSMAC, cSMAC, and pSMAC/cSMAC junction is plotted below the images as described in Figure 1A. At least 20 IS forming cells were analyzed for each time point in 2 independent experiments.

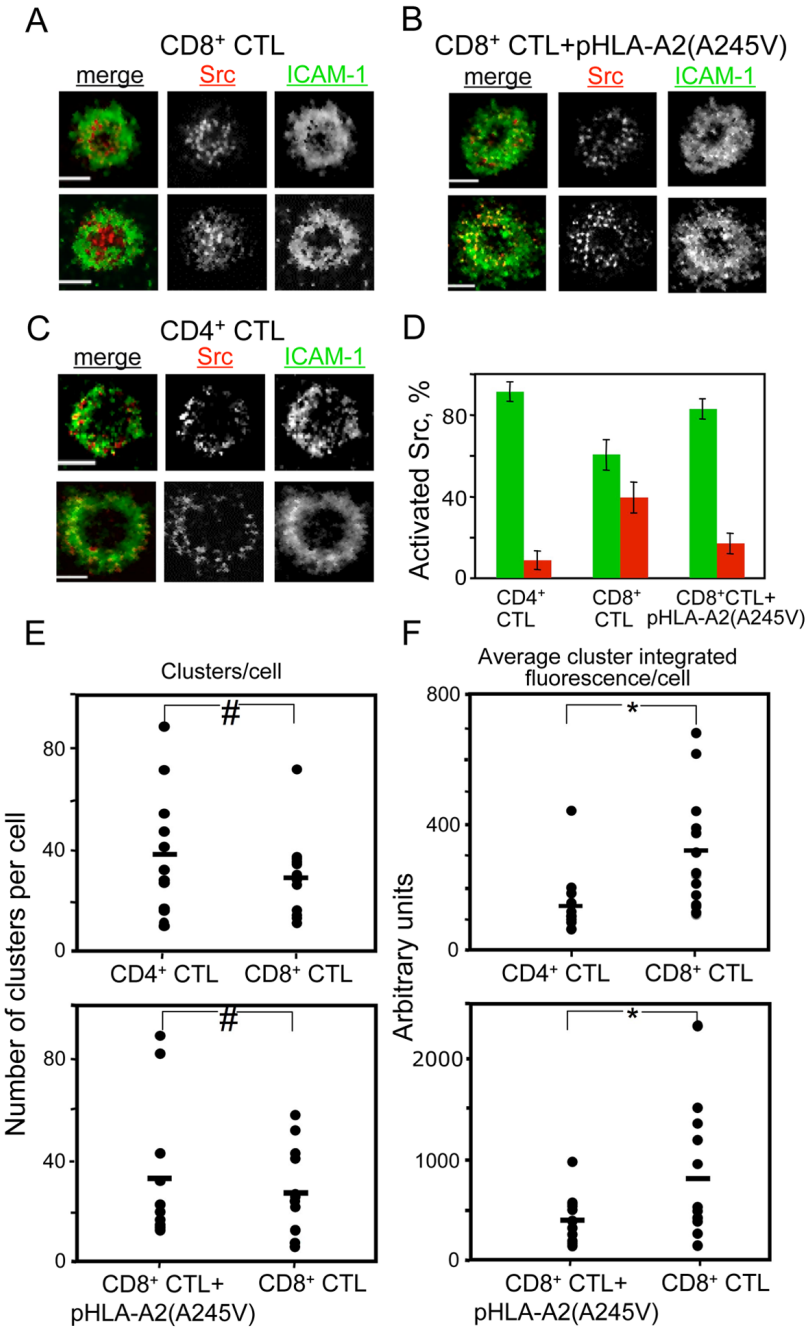

Figure 2. Similarities and differences in TCR-mediated signaling in CTL exercising more and less effective cytolytic responses

Representative TIRF images of $CD8^+$ CTL interacting with ICAM-1-containing bilayers that display either intact cognate pHLA-A2 (**A**) or the pHLA-A2(A245V) molecules (**B**) or $CD4^+$ CTL contacting the bilayers with cognate pMHC-II proteins (**C**) are shown. ICAM-1 is green, and activated Src kinases are red. Scale bar: 5μm. (**D**) The percentage of the fluorescence signal of the phospho-Src kinases in the pSMAC (green) and the cSMAC (red) is depicted as a bar diagram. The data are from analysis of at least 48 IS-forming cells of 2 independent experiments. The number of signaling clusters (**E**) and the amount of activated Src kinases per cluster (**F**) at the synapse formed by $CD8^+$ and $CD4^+$ CTL. Top panels: Comparison of

$CD4^+$ and $CD8^+$ CTL exposed to bilayers containing respective cognate pMHC complexes and ICAM-1. Bottom panels: Comparison of $CD8^+$ CTL CER43 exposed to bilayers containing either intact cognate GL9-HLA-A2 or GL9-HLA-A2(A245V) complexes plus ICAM-1. Data shown is from 12 IS-forming cells. Statistical analysis was performed by Student's *t*-tests for paired data. #: $P>0.25$, *: $P\leq0.05$.

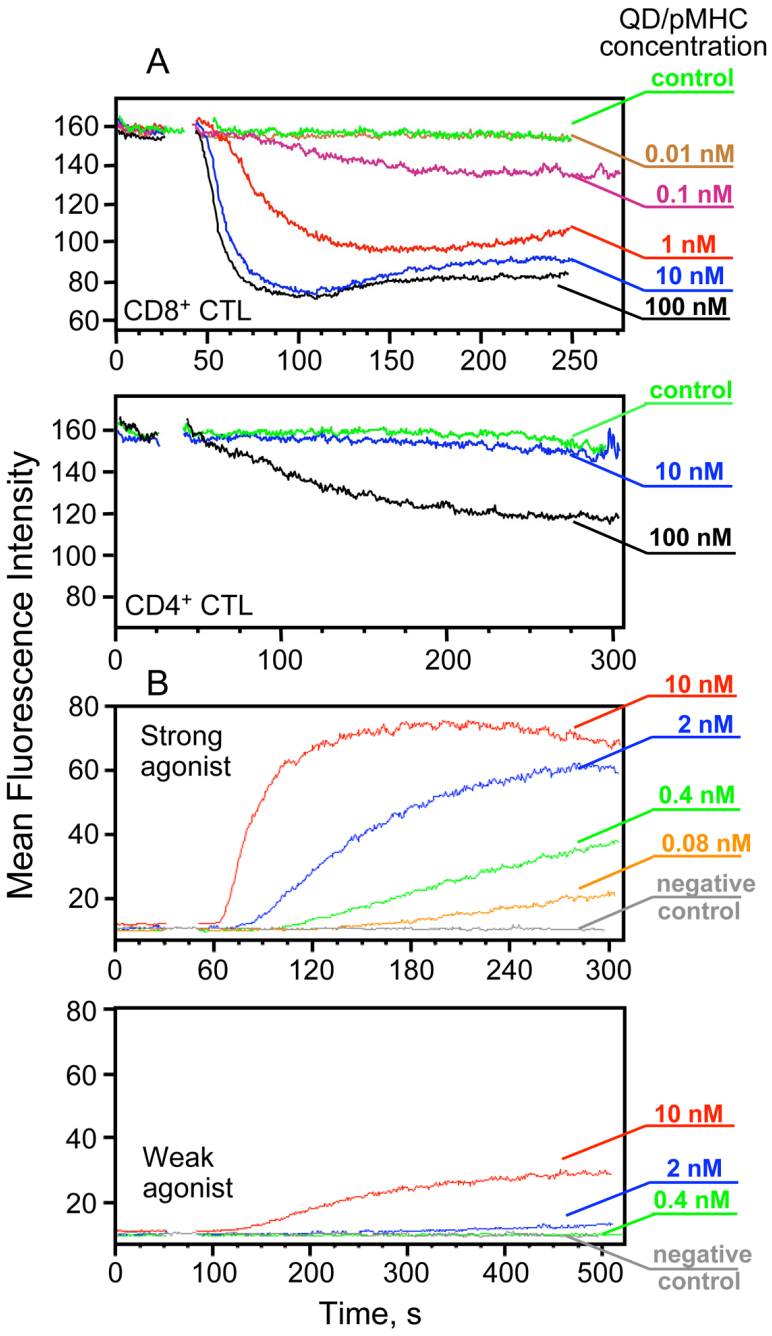

Figure 3. Difference in the kinetics of early signaling in CD8$^+$ and CD4$^+$ CTL

(**A**) Time-dependent changes in intracellular calcium concentration in CER43 CD8$^+$ CTL (top panel) and AC-25 CD4$^+$ CTL (bottom panel) induced by cognate QD-520/GL9-HLA-A2 and QD-520/PP16-DR1 conjugates, respectively, at indicated concentrations. Controls (green) show changes in intracellular calcium in the CTL in the presence of 100 nM of non-cognate QD-520/pMHC conjugates. The results of representative experiments are shown.

(**B**) Difference in the kinetics and magnitude of Ca^{2+} flux in 68A62 CD8$^+$ CTL induced by QD-620 bearing either strong (IV9-HLA-A2, top panel) or weak (IV9-A7-HLA-A2, bottom panel) agonists at indicated concentrations. The results of representative experiments are shown.

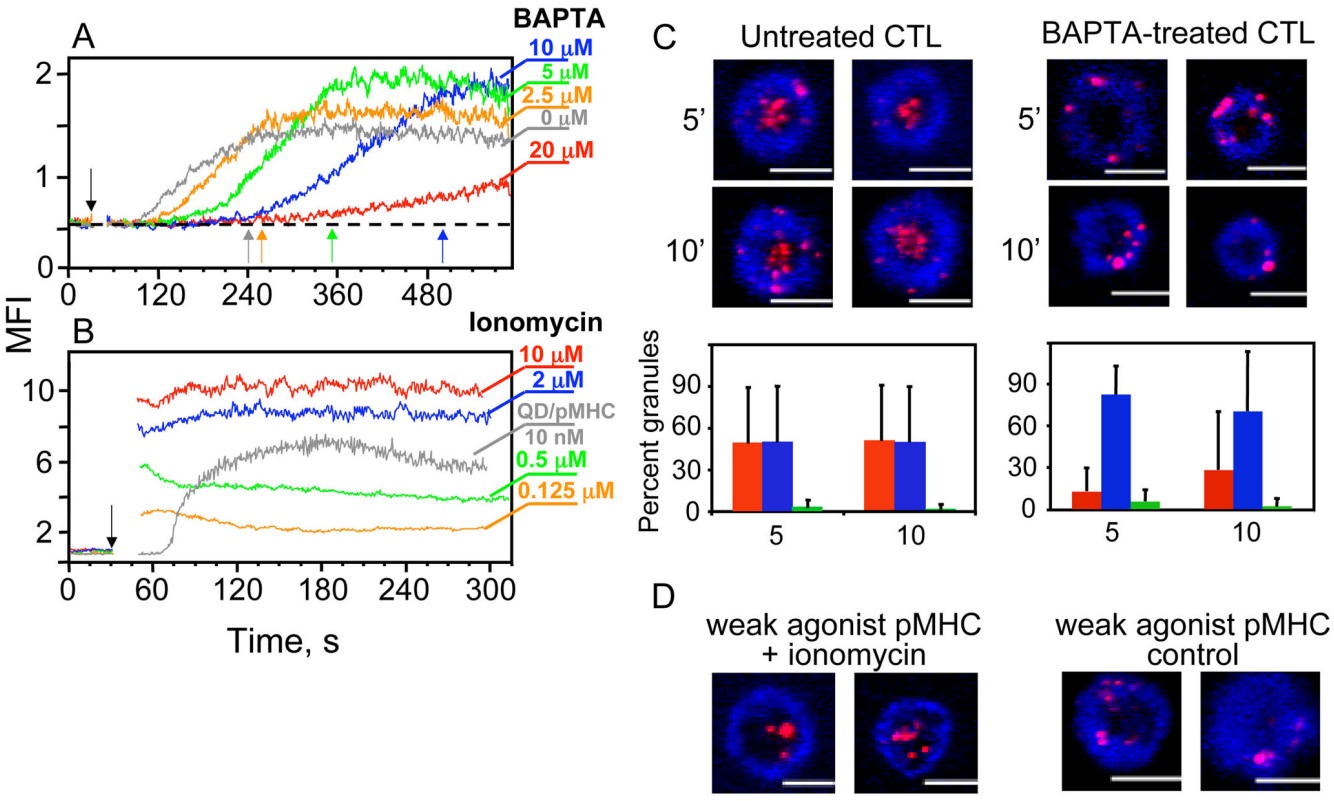

Figure 4. Effect of receptor-independent alterations in intracellular calcium accumulation on the distribution of granules at the cytolytic synapses

(**A**) BAPTA treatment of $CD8^+$ CTL prior to stimulation with QD-620 bearing strong agonist pMHC ligands significantly delayed the kinetics of intracellular Ca^{2+} accumulation. Black arrow indicates time points at which QD/pMHCs were added. Colored arrows indicate the times at which Ca^{2+} flux approached maximum at various BAPTA concentrations (depicted in the panel). (**B**) Ionomycin rapidly induces calcium influx in $CD8^+$ CTL in a dose-dependent manner. Ionomycine concentrations are indicated. Ca^{2+} flux induced by cognate QD(620)/pMHC conjugates at 10 nM is shown as a positive control. Black arrow indicates time point at which ionomycin or QD/pMHCs were added. (**C**) Treatment with BAPTA at 10 μM significantly decreased the amount of granules in the cSMAC of 68A62 $CD8^+$ CTL on bilayers containing ICAM-1 and strong agonist pMHC (IV9-HLA-A2) at 25 molecules/μm^2 (upper panels). ICAM-1 is blue and granules are red. Scale bar: 5μm. The percentage of granules localized in the pSMAC (blue), cSMAC (red), and pSMAC/cSMAC junction (green) at the bilayer level is shown at the bottom panel. At least 10 IS forming cells from 2 independent experiments at the indicated time points were analyzed. (**D**) Stimulation of 68A62 $CD8^+$ CTL exposed to ICAM-1-containing bilayers with IV9-A7-HLA-A2 weak agonist at 1 μM plus 1 μM ionomycin resulted in repositioning of the polarized granules to the cSMAC of the synapse. Representative images of two cells show granule positioning (red) relative to the ring junction (blue) in 68A62 $CD8^+$ CTL in the presence (left panel) or absence (right panel) of ionomycin. At least 15 cells of each category from 2 independent experiments were analyzed. Scale bar: 5μm.

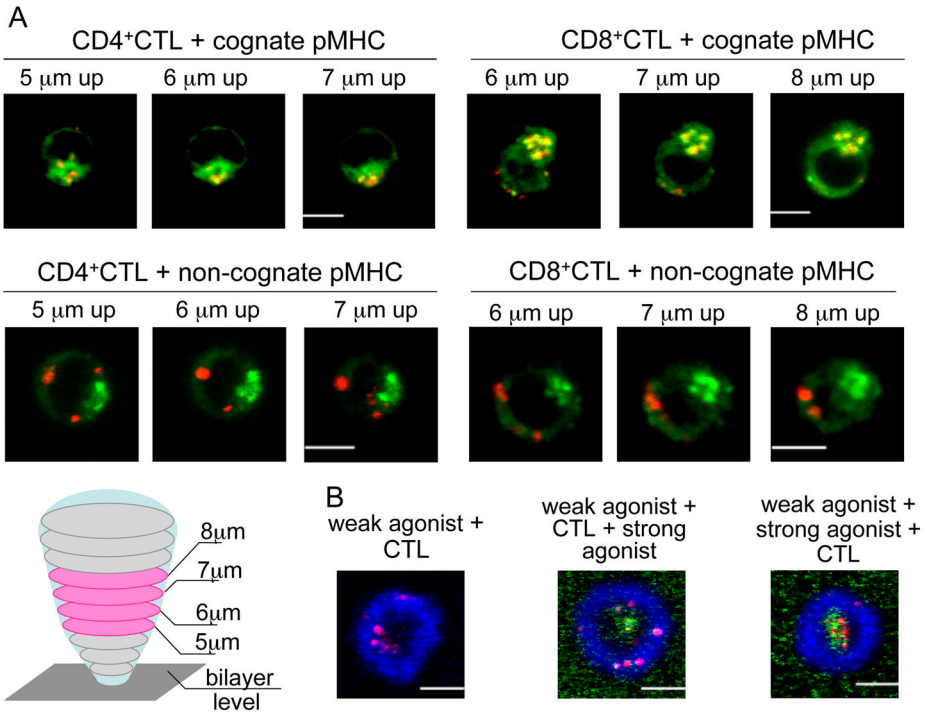

Figure 5. Temporal balance between the two principal movements determines the granule polarization pattern

(**A**). Representative images of granules (red) and Golgi complex (green) in AC-25 $CD4^+$ and CER43 $CD8^+$ CTL interacting with bilayers containing either cognate or non-cognate pMHC alone are shown. Three sequential z-stack images located in the middle of the cells, in which the Golgi complex staining was most prominent, are shown for each CTL. The majority of $CD4^+$ and $CD8^+$ CTL (50–70%) exposed to cognate pMHC concentrate most of their granules near the Golgi complex (top images), while 85–90% of the CTL exposed to non-cognate pMHC do not (bottom images). Scale bar: 5 μm. A cartoon depicts the CTL interacting with a bilayer containing cognate pMHC proteins only. Z-sections were acquired at 1 μm intervals through the cell volume beginning at the bilayer level. The MTOC location in the middle sections indicates that the MTOC was not polarized.

(**B**). Increasing the strength of TCR stimulation after mature synapse formation does not promote granule accumulation in the cSMAC. Polarized granules (red) in 68A62 $CD8^+$ CTL exposed to bilayers containing unlabeled weak agonist pMHC (500 molecules/μm^2) and ICAM-1 (blue) are recruited to the periphery of the cytolytic synapse (left panel). Alexa Fluor 488-labeled strong agonist pMHC (green) was then flowed into the bilayers at 1 μM and accumulated in the cSMAC, but failed to induce the central location of polarized granules (middle panel). In control experiments, CTL exposure to bilayers that were initially loaded with weak agonist pMHC and ICAM-1 and then modified by the addition of strong agonist pMHC resulted in the recruitment of the strong agonist and the granules to the cSMAC (right panel). One representative cell of 9–12 analyzed cells in each category from 2 experiments is shown. Scale bar 5 μm.

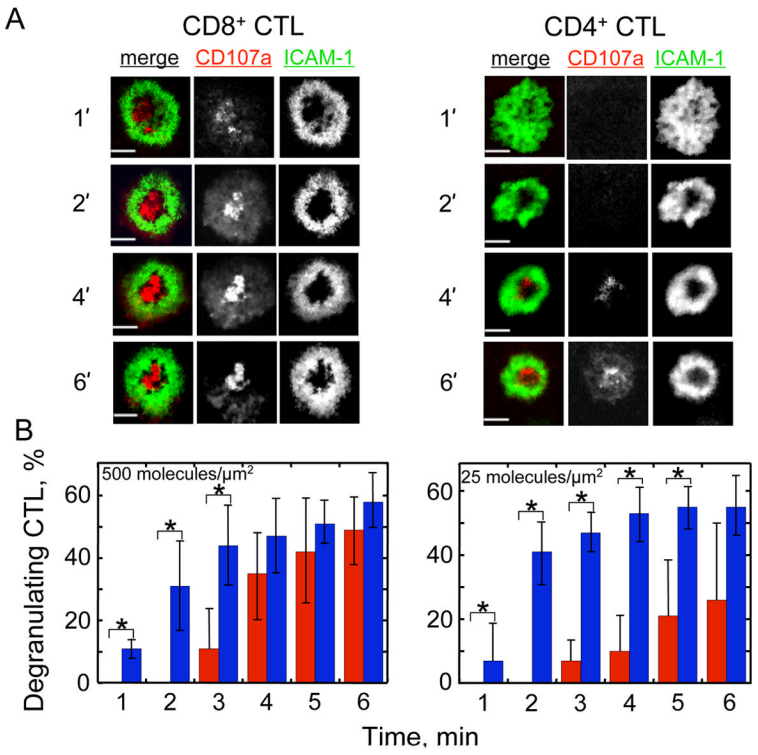

Figure 6. Kinetics of granule release into the secretory domain of more ($CD8^+$) and less ($CD4^+$) effective CTL

(**A**) Representative TIRF images of a CER43 $CD8^+$ and AC-25 $CD4^+$ CTL interacting with bilayers containing the respective cognate pMHC proteins demonstrate the difference in the kinetics of granule release. Granules (CD107a): red, ICAM-1: green. Scale bar: 5μm. (**B**) The graphs show the percentage of CD107a positive CTL interacting with bilayers containing ICAM-1 and cognate pMHC at a density of either 500 molecules/μm^2 (left) or 25 molecules/μm^2 (right) as a function of time. Blue: $CD8^+$ CTL, red: $CD4^+$ CTL. More than 20 cells from at least 2 independent experiments were analyzed in each case. Statistical analysis was performed by Student's *t*-tests. *: $P<0.05$.

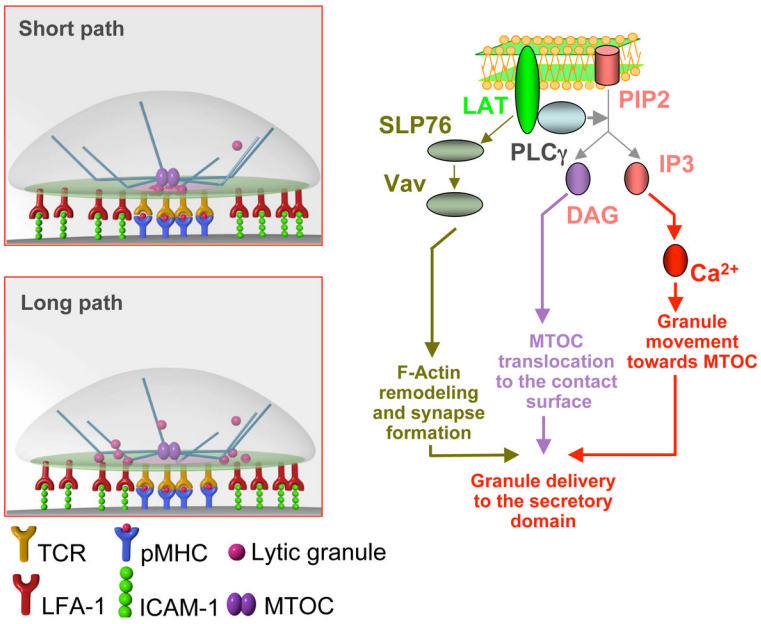

Figure 7. Downstream Ca^{2+}-dependent signaling influences the balance between the long and the short paths of granule delivery

The stronger early TCR signaling is initiated by a greater number of activated signaling proteins per microcluster and leads to rapid kinetics of intracellular Ca^{2+} accumulation, while a weaker early signaling does not. Rising the concentration of intracellular Ca^{2+} results in the activation of downstream signaling that regulates granule movement to the MTOC. In contrast, MTOC translocation is Ca^{2+}-independent and is primarily mediated by DAG-dependent signaling. A faster Ca^{2+} signaling in more effective CTL stimulates swift granule movement towards the MTOC and the granules are concentrated near the MTOC prior to MTOC polarization. The MTOC then directly delivers granules to the secretory domain – the short path. A slower Ca^{2+} signaling in less effective CTL results in a delay in granule recruitment and granules move along the microtubules to the periphery of the synapse looping through the pSMAC – a longer path. MTOC polarization to the mature synapse also requires F-actin remodeling and segregation as well as the recruitment of ADAP-associated dynein to the periphery of the actin ring. Vav-dependent downstream signaling plays a critical role in regulating these molecular events. Cartoons at the upper and bottom left are courtesy of Christoph Schmutte.